Jurnal Ilmiah Teknik Elektro Komputer dan Informatika (JITEKI)
Vol. 10, No. 3, September 2024, pp. 566-579
ISSN: 2338-3070, DOI: 10.26555/jiteki.v10i3.29601

Image-Based Position Control for Three-Wheel Omni-Directional Robot

Sri Sukamta, Anan Nugroho, Subiyanto, Rizal Rezianto, Muhammad Febrian Soambaton, Agus Ardiyanto
Universitas Negeri Semarang, Sekaran Gunung Pati, Semarang, Jawa Tengah, 50229, Indonesia

ARTICLE INFO

Article history:

Received July 25, 2024
Revised August 30, 2024
Published September 14, 2024

Keywords:

Image Based Control;
Infrared Sensor;
Waypoint Navigation;
Omni-Directional Wheels;
Mobile Robots

ABSTRACT

Robotic technology continues to advance, but real-time position tracking of robot movements still faces challenges, especially in dynamic and irregular environments. Sensors often fail to maintain accuracy due to environmental disturbances. This study introduces an innovation using omnidirectional wheels on a three-wheeled robot and image-based position control to improve maneuverability and precision. This method utilizes an infrared camera mounted on the ceiling to detect the robot's position. Image processing algorithms are used to determine waypoints and direct the robot. Omni-directional wheels allow the robot to move freely in all directions, which is important for accurate navigation on complex trajectories. The robot was tested on the "X" and "Square" trajectories in a 1.8-meter x 1.8-meter room to rotate vertical, horizontal, and diagonal movements. The test results showed that on the "X" trajectory, the second movement had the most significant error with a Mean Absolute Error (MAE) of 134.96, while the third movement had the slightest error with an MAE of 52.49, with an average error of 91.36. The first and third movements in the “Square” trajectory showed more significant errors than the second and fourth movements, with MAE of 105.37 and 100.47, respectively. The second and fourth movements had MAE of 67.20 and 59.65, with an average error of 83.17. These results indicate that the image-based control system and omnidirectional wheels improve accuracy compared to conventional methods, which is important for robot navigation applications. Practical implications of this technology include potential applications in the robotics and automation industry. Future research should focus on developing more precise control algorithms and sensors to improve accuracy. Directions for future research include exploring more sophisticated image processing techniques and applying this technology to various industrial scenarios.

Corresponding Author:

Sri Sukamta, Universitas Negeri Semarang, Sekaran Gunung Pati, Semarang, Jawa Tengah, 50229, Indonesia
Email: ssukamta2014@mail.unnes.ac.id

1. INTRODUCTION

Technology is progressing rapidly, especially in the context of robot development. The use of sensors in robot development is necessary so that robots can comply with the instructions [1], [2]. The application of robots in industry to increase productivity depends on work models that are relatively routine, simple, and require low skills [3], [4]. Although real-time tracking capabilities are easy for humans, animals, and other living creatures in dynamic areas, this is not the case for mobile robots [5], [6]. Recent research shows that the detection and tracking of moving objects in dynamic environments often suffer from velocity estimation errors and occlusion problems [7], [8]. In addition, LiDAR-based obstacle detection and tracking reveals significant challenges in distinguishing between static and dynamic objects and overcoming obstacles in the robot's path [9]. Conventional sensors, such as LiDAR, often cannot provide accurate information about objects in the

robot's path, especially in highly dynamic environments [10]. This gap indicates the need for more effective approaches to detect and track objects with higher precision.

Large companies implementing automation, including robots, can increase productivity and labor costs over time [11]. Stationary industrial robots have high precision but often do not reach their goals precisely due to rough or irregular environments [12], [13], [14]. Omnidirectional wheels can significantly increase maneuverability [15]. Robots with omnidirectional wheels can move in all directions; with a mathematical kinematics model, the robot performs vector analysis of the speed and direction of movement of each omnidirectional wheel [16], [17]. Robots implementing omnidirectional movement have good maneuverability and flexibility to increase mobility in confined spaces [18], [19].

Omnidirectional wheels allow the robot to have a holonomic character, which means it can move in any trajectory without direction restrictions [20]. Robots with three omnidirectional wheels can move in any direction from any position because the wheelbase allows unrestricted maneuvering [21], [22], [23]. In this context, the development of kinematic models and the application of control algorithms such as PID are expected to improve the stability and accuracy of robot movements [24], [25], [26].

Visual cameras are a particularly popular choice for robot control utilizing the limited onboard sensing that is available since they can deliver richer information at a cheaper cost when compared to other standard sensors [27], [28]. To support this capability, the control method uses image-based position control for a mobile robot with a fixed camera mounted on the ceiling. The advantage of this method lies in the simplicity of the controller design, which does not require detailed knowledge of intrinsic (such as focal length and lens distortion) and extrinsic (such as camera position and orientation relative to the observed object) parameters [29]. Using visual feedback from cameras can significantly improve the efficiency and accuracy of robot control in precision manipulation tasks [30], [31]. Direct visual control methods using information from images captured by cameras can avoid camera calibration problems and offer higher responsiveness in robot control, so these systems can be easily adapted for various types of practical applications [32], [33]. cameras have intrinsic, extrinsic, and distortion parameters. This aspect can adjust the intended kinematic model according to the two specific additional feature points [34], [35].

Using uncalibrated cameras for robot formation control can reduce performance degradation caused by calibration inaccuracies [36]. Another advantage is that cameras with limited field-of-view (FOV) can provide a low-cost, easy-to-implement solution for mobile robot formation control [37]. This allows using a relatively simple controller with visual feedback of the image measured by the onboard camera, offering robustness to model uncertainty without requiring in-depth information about feature depth and leader speed [38].

In this context, no research specifically combines the use of omnidirectional wheeled robots with image-based position control. This study aims to fill this gap by exploring the potential integration between the superior maneuverability of omnidirectional wheeled robots and the visual control capabilities using cameras. Thus, this research is expected to significantly contribute to developing modern robotics technology that is more responsive and adaptive to the surrounding environment, with the potential for broader application in various industries.

2. METHODS

This research tests the performance of implementing image-based position control on a Three-Wheel Omni-Directional Robot using waypoints to determine the destination point. The research flow in this study begins with identifying problems related to the robot navigation system. Next, a literature review is conducted to understand existing methods and technologies (Fig. 1). This review divides the research into two main paths: robot control strategies and control parameters. Robot control strategies focus on the approaches used to move the robot effectively, while control parameters relate to the variables that affect system performance. Following this path, a research method is designed to integrate the control strategies and parameters that have been determined. The next stage is experimentation and analysis, where the robot is tested on the 'X' and 'Square' trajectories to assess the system's ability to manage complex movements. The results of these experiments are then analyzed in depth to determine the system's effectiveness. This study ends with a conclusion that summarizes the main findings and provides recommendations for further development.

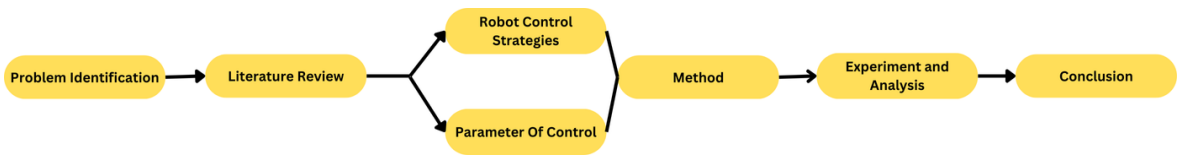

Fig. 1. Methods

The flowchart of a robotic system is shown in Fig. 2, including the control of the robot to achieve the goal and the kinematics of the three omnidirectional robots, both of which will be explained in the next section to provide an understanding of the research process.

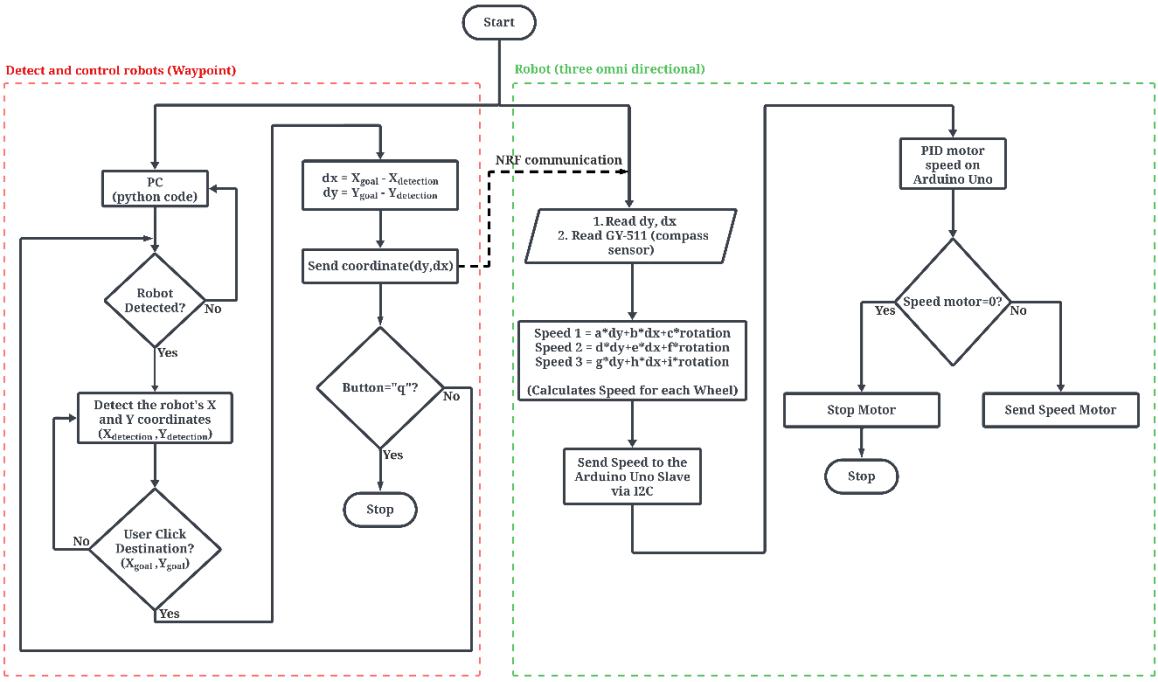

Fig. 2. System Flowchart

Based on Fig. 2, the system flowchart is divided into two main sections: robot detection and navigation control and omnidirectional robot control. In the first section, the computer receives input from a camera that provides a live image stream of the area where the robot is located. The Python code processes this image to distinguish the robot from other objects in the area, allowing the robot to be detected. The Python code also detects the robot's coordinates based on its position within the area. If the user clicks on a point in the area, the computer sends the coordinates of the selected destination to the second section, which handles the omnidirectional robot control. If the user does not click on anything, the program loops back to continue detecting the robot's coordinates. In the second section, the robot receives the destination coordinates via the microcontroller. These coordinates are then processed according to the robot's kinematics to determine the appropriate motor speeds for each wheel, enabling the robot to move toward the destination. As the robot moves, the camera continuously monitors its movement and updates the robot on the correct path to take. When the robot reaches the destination determined by subtracting the current coordinates from the target coordinates and achieving a result of zero, the computer sends a (0,0) coordinate signal to the robot, instructing it to stop at the destination.

2.1. Robot Detection and Waypoint Navigation

To get information about the robot's position, when the robot is walking on the road, it also needs to recognize the road area using object detection [39]. For the robot to reach its goal, navigation is required. A waypoint is a reference point or set of coordinates used for navigation purposes to identify a point in a mapping area [40], [41], [42]. When a robot must go toward a preset destination, it is called a waypoint. To save costs and boost profits, the industry places a high value on productivity and efficiency [43]. In this research, area mapping was carried out by a camera that detected the area below shown in Fig. 3.

Robot detection results require a threshold value set based on ambient light conditions assisted by an external filter on the camera lens. A camera's "threshold value" refers to the contrast level used for image processing. A higher threshold value results in higher image contrast, making the image have more distinct differences between different colours. When using an infrared (IR) pass filter on the camera, the three dots employed as indicators on the robot become more distinct from other light sources. The threshold value is adjusted according to the ambient light conditions in the room. A higher threshold value may be necessary in environments with strong external IR sources, such as sunlight. The camera uses a Hikvision ds-2cd1021-i

with the ability to capture infrared light in night mode. This camera was chosen because of the IR pass capability on the camera and the high resolution of 1920 × 1080. Still, this camera has a wide lens, horizontal FOV of 114.8°, vertical FOV of 62° and diagonal FOV: 135.5° which makes the camera view convex without any lens settings camera.

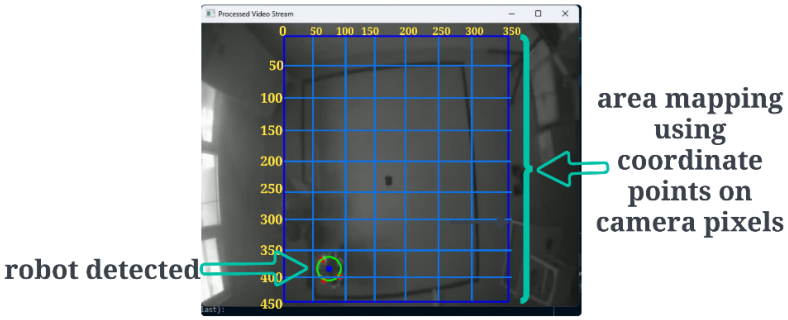

Fig. 3. Mapping area and Robot Detected

This result was acquired in a closed room to test robot movements with lighting conditions of 7 to 10 lux, resulting in a threshold value of 192 to 200 (Fig. 4). A threshold value of 200 was chosen because it provided the best contrast, effectively isolating the three dots on the robot from other light sources in the experimental room. The detection process involves processing the image captured by the camera, where only white pixels are extracted. The contrast is then manually fine-tuned so that the only visible white sources are the three dots on the robot, allowing for accurate robot detection. However, this method has a limitation: the robot may not be appropriately detected if an external light source is brighter than the three dots. To address this issue, an additional criterion is applied—the distance between each dot must not exceed a specific value based on the known distance between the three dots on the robot. The camera will detect that the three dots are robots and pinpoint the coordinates from the center in the middle.

Waypoints generate trajectories that avoid interference and allow the robot to choose the best path [44], [45]. The robot motion formula in this context calculates the relative displacement required to direct the robot from its current position to the point clicked by the user (Fig. 5).

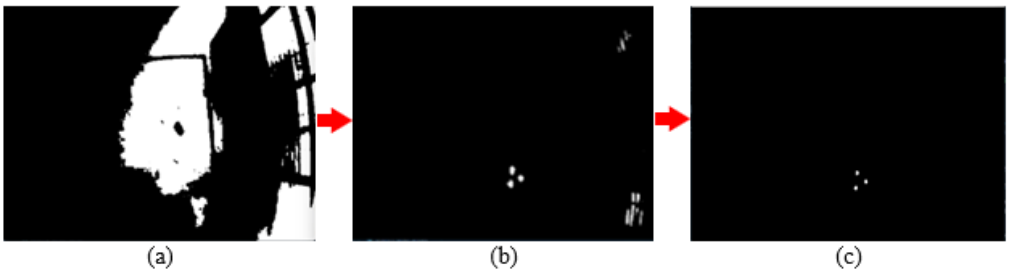

Fig. 4. (a) Threshold value of 20; (b) Threshold value of 100; (c) Threshold value of 200

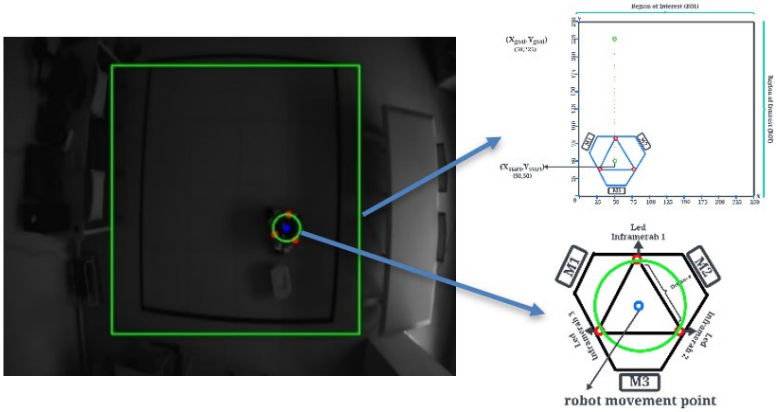

Fig. 5. Robot Work Area Can Be Detected

Horizontal displacement (dx) is calculated by subtracting the x coordinate of the clicked point from the robot's current x coordinate. Meanwhile, vertical displacement (dy) is calculated by subtracting the y coordinate of the clicked point from the robot's current y coordinate.

$$dx = (X_{\text{clicked}} - X_{\text{current}}) \quad (1)$$

$$dy = (Y_{clicked} - Y_{current}) \quad (2)$$

where $X_{\text{clicked}}, Y_{\text{clicked}}$ are the coordinates of the point clicked by the user and $X_{\text{current}}, Y_{\text{current}}$ is the current position of the robot. With an illustration of the robot in Fig. 6. The results of these calculations are then used to send movement commands to the Robot, which allows the user to interactively control the robot's movement according to the selected position in the monitored environment.

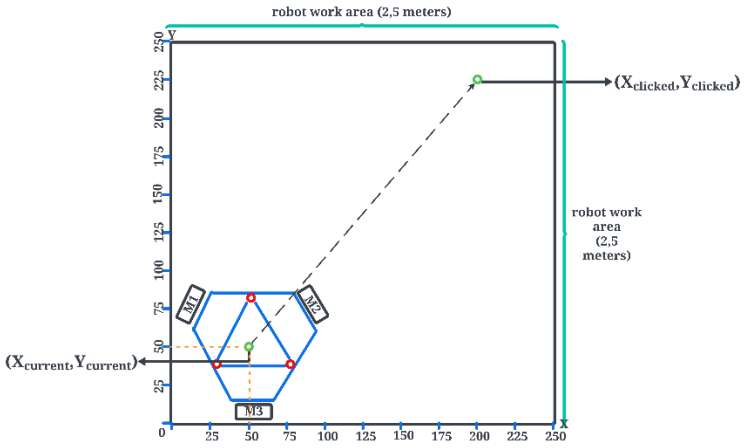

Fig. 6. Robot Work Area

2.2. Kinematic Three Omni-Directional Robot

The movement of this robot uses three omnidirectional wheel kinematics models [46]. The kinematic model is crucial to quantitatively describe how a mobile robot operates. It also makes it possible to connect the robot's motion to the speed of its motor units or the actuators that drive its propulsion and movement [47], [48]. The wheels are placed on three radius of a circle that have an angle of 120° from each other while the center of the circle becomes the robot coordinates [49], [50]. The placing of wheels, the velocity vector of each wheel, and the robot's global axis coordinate shown in Fig. 7.

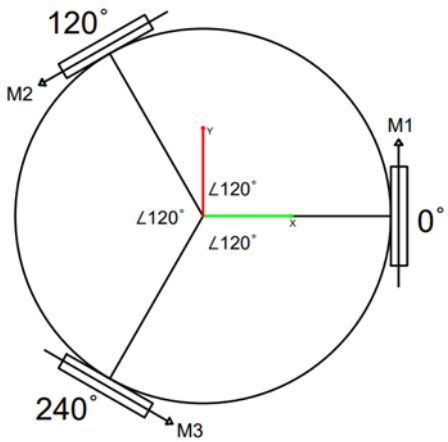

Fig. 7. The placing of wheels, the velocity vector of each wheel, and the robot's global axis coordinate

From the velocity of vectors M1, M2, and M3. The overall movement of the robot on the global axis is the sum of each velocity vector that can be represented (3) [17].

$$\overrightarrow{F_o} = \overrightarrow{F_{M1}} + \overrightarrow{F_{M2}} + \overrightarrow{F_{M3}} \quad (3)$$

The vector above has its components: the x component and the y component. The given components are given (4) and (5). The vector component for each wheel is given in the representation Fig. 8.

$$\overrightarrow{Fx} = \overrightarrow{Fx_{M1}} + \overrightarrow{Fx_{M2}} + \overrightarrow{Fx_{M3}} \quad (4)$$

$$\overrightarrow{Fy} = \overrightarrow{Fy_{M1}} + \overrightarrow{Fy_{M2}} + \overrightarrow{Fy_{M3}} \quad (5)$$

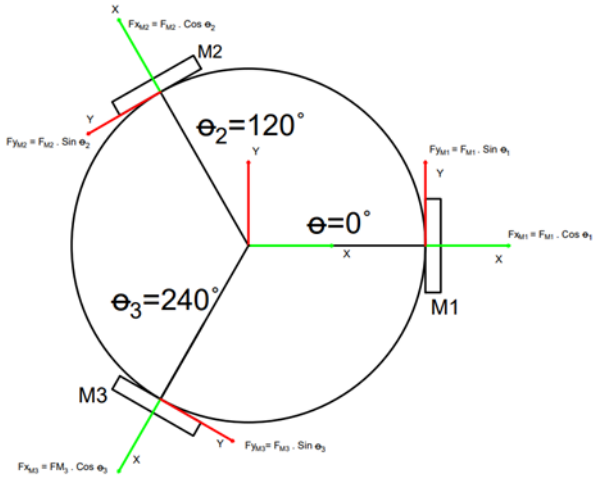

Fig. 8. Vector of each wheel

From equation (4) the $\overrightarrow{Fx_{M1}}$, $\overrightarrow{Fx_{M2}}$, and $\overrightarrow{Fx_{M3}}$ are changed to $\overrightarrow{F_{M1}}.\boldsymbol{Cos\ \theta_1}$, $\overrightarrow{F_{M2}}.\boldsymbol{Cos\ \theta_2}$, and $\overrightarrow{F_{M3}}.\boldsymbol{Cos\ \theta_3}$ with $\overrightarrow{F_{M1}}$, $\overrightarrow{F_{M2}}$, and $\overrightarrow{F_{M3}}$ as a motor velocity and $\boldsymbol{\theta_1}$, $\boldsymbol{\theta_2}$, and $\boldsymbol{\theta_3}$ as angle of the radians which the wheel placed in this proposed system the angle is assumed to be 0°, 120°,240°. Same as the equation (4), equation (5) is changed to its respected vector, the updated equation is shown in (6) and (7).

$$\overrightarrow{Fx} = \overrightarrow{F_{M1}}.\boldsymbol{Cos\ \theta_1} + \overrightarrow{F_{M2}}.\boldsymbol{Cos\ \theta_2} + \overrightarrow{F_{M3}}.\boldsymbol{Cos\ \theta_3} \quad (6)$$

$$\overrightarrow{Fy} = \overrightarrow{F_{M1}}.\boldsymbol{Sin\ \theta_1} + \overrightarrow{F_{M2}}.\boldsymbol{Sin\ \theta_2} + \overrightarrow{F_{M3}}.\boldsymbol{Sin\ \theta_3} \quad (7)$$

The equation using different $\boldsymbol{\theta_1}$, $\boldsymbol{\theta_2}$, and $\boldsymbol{\theta_3}$ is due to the rotation of the radian. While equations (6) and (7) are linear movement, the three omnidirectional wheels have also rotating movement, the rotating movement is shown (8).

$$\overrightarrow{Fr} = \overrightarrow{F_{M1}} + \overrightarrow{F_{M2}} + \overrightarrow{F_{M3}} \quad (8)$$

The three-motor velocity vector is 90° to the center of the circle, with the same motor velocity and direction, making the robot perform a circular motion. Equations (6), (7), and (8) are then changed to their matrix form for inversing the kinematics [51]-[54].

$$\begin{bmatrix} \overrightarrow{Fx} \\ \overrightarrow{Fy} \\ \overrightarrow{Fr} \end{bmatrix} = \begin{bmatrix} \boldsymbol{Cos\ \theta_1} & \boldsymbol{Cos\ \theta_2} & \boldsymbol{Cos\ \theta_3} \\ \boldsymbol{Sin\ \theta_1} & \boldsymbol{Sin\ \theta_1} & \boldsymbol{Sin\ \theta_1} \\ \boldsymbol{1} & \boldsymbol{1} & \boldsymbol{1} \end{bmatrix} \times \begin{bmatrix} \overrightarrow{F_{M1}} \\ \overrightarrow{F_{M2}} \\ \overrightarrow{F_{M3}} \end{bmatrix} \quad (9)$$

$$\begin{bmatrix} \overrightarrow{F_{M1}} \\ \overrightarrow{F_{M2}} \\ \overrightarrow{F_{M3}} \end{bmatrix} = \begin{bmatrix} \boldsymbol{Cos\ \theta_1} & \boldsymbol{Cos\ \theta_2} & \boldsymbol{Cos\ \theta_3} \\ \boldsymbol{Sin\ \theta_1} & \boldsymbol{Sin\ \theta_1} & \boldsymbol{Sin\ \theta_1} \\ \boldsymbol{1} & \boldsymbol{1} & \boldsymbol{1} \end{bmatrix}^{-1} \times \begin{bmatrix} \overrightarrow{Fx} \\ \overrightarrow{Fy} \\ \overrightarrow{Fr} \end{bmatrix} \quad (10)$$

From equation (10), all the thetas are changed to $\boldsymbol{\theta + \theta_H}$ with $\boldsymbol{\theta_H}$ as the rotated heading in the global compass, so the robot can be placed at any heading angle and still move in the desired direction. Heading rotation changing the initial angle by θ_H shown in Fig. 9.

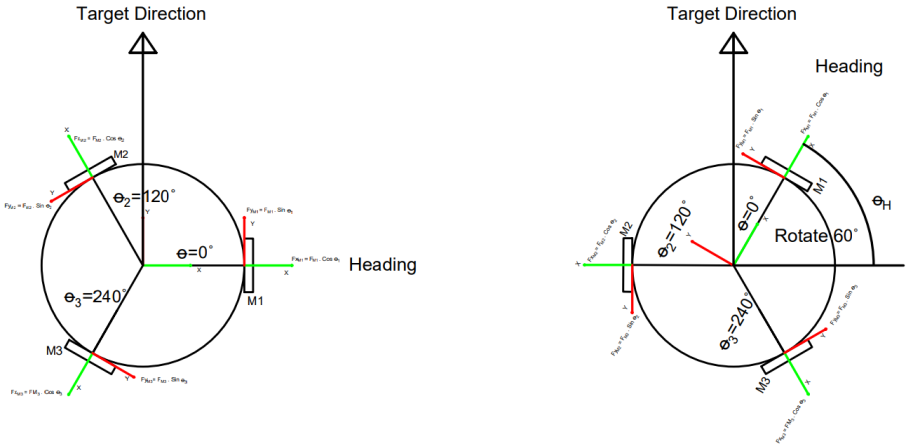

Fig. 9. Heading rotation changing the initial angle by θ_H

$$\begin{bmatrix} \overrightarrow{F_{M1}} \\ \overrightarrow{F_{M2}} \\ \overrightarrow{F_{M3}} \end{bmatrix} = \begin{bmatrix} Cos\,(\theta_1+\theta_H) & Cos\,(\theta_2+\theta_H) & Cos\,(\theta_3+\theta_H) \\ Sin\,(\theta_1+\theta_H) & Sin\,(\theta_2+\theta_H) & Sin\,(\theta_1+\theta_H) \\ 1 & 1 & 1 \end{bmatrix}^{-1} \times \begin{bmatrix} \overrightarrow{Fx} \\ \overrightarrow{Fy} \\ \overrightarrow{Fr} \end{bmatrix} \quad (11)$$

The equation (11) above can generate motor speed velocity for each motor in given x and y vectors. The robot's motor speed is controlled using a Proportional-Integral-Derivative (PID) control algorithm, which was selected for its simplicity in microcontroller implementation [55]. The PID parameters were tuned using a trial-and-error approach, where different P, I, and D values were tested and the output analyzed. The proportional (P) gain was reduced if the output graph exhibited an overshoot. If the stabilization time was too long, the integral (I) gain was increased. In cases of undershoot, the proportional gain was increased, and the derivative (D) gain was adjusted to reduce overshoot [55]. The PID equation is shown in (12) [56], [57], [58].

$$y(t) = K_p e(t) + K_i \int e(t)\,dt + K_d \frac{de}{dt} \quad (12)$$

The $y(t)$ are the output while K_p, K_i, and K_d are the proportional gain, integral gain, and deferential gain with e as the error from target and the output.

3. RESULTS AND DISCUSSION

This paper presents the results of experiments evaluating a robot's movement performance following a straight track, aiming to achieve precise control using a visual infrared camera for robot detection. The testing was conducted by navigating the robot along predefined waypoints, with several experiments varying the starting and destination points to assess the waypoint navigation system's performance under the control of the visual infrared camera. The experimental setup took place in a room with a lighting level of 7 - 10 and a smooth surface. The tests involved two primary paths: a square route and an X-shaped route, designed to evaluate the robot's navigational ability along diagonal, horizontal, and vertical axes. Data were collected using the same visual infrared camera to detect the robot's coordinates. These coordinates were then saved and analyzed by comparing the software-generated waypoints with the actual waypoints to identify errors in the navigation system. PID output graph shown in Fig. 10.

This graph represents the outcome of manual PID tuning for three motors, with the following PID parameters: Motor 3 (Kp = 0.42, Ki = 7, Kd = 0.03), Motor 2 (Kp = 0.3, Ki = 6, Kd = 0.03), and Motor 1 (Kp = 0.3, Ki = 5.5, Kd = 0.03). These values were selected because they provided the optimal output based on experimental results. The robot was tested to evaluate the differences between the expected and actual movement paths within a controlled environment measuring 1.8 meters by 1.8 meters. The tests involved horizontal, vertical, and diagonal movements, forming two specific patterns: a "square" and an "X." Each pattern included four different starting and destination points, creating straight-line trajectories.

In the "X" pattern, as shown in Fig. 11, the movement was divided into four segments: (1) a short diagonal from the center to the top-right corner, (2) a long diagonal from the top-right to the bottom-left corner, (3) a short diagonal from the center to the top-left corner, and (4) a long diagonal from the top-left to the bottom-right corner. The robot's path was recorded and represented by a red line, while the expected path was shown

in blue in Fig. 10. The overall average error for the "X" pattern was 91.36 pixels, equivalent to an 18.53% deviation from the path generated by the software.

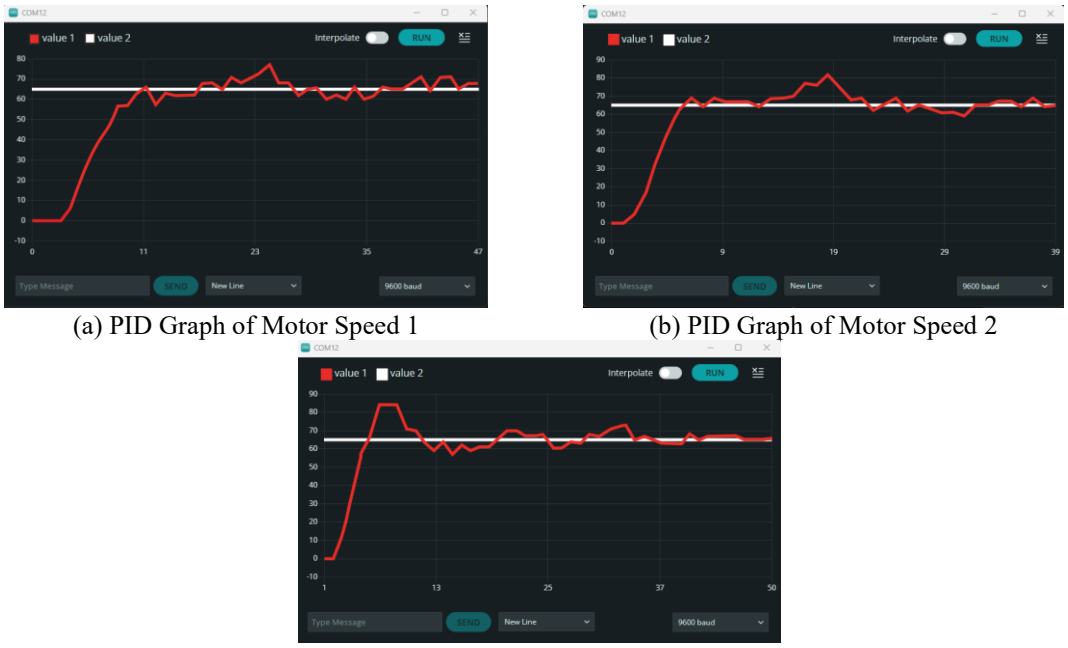

(a) PID Graph of Motor Speed 1 (b) PID Graph of Motor Speed 2

(c) PID Graph of Motor Speed 3

Fig. 10. (a) PID output graph at motor speed 1; (b) PID output graph at motor speed 2; (c) PID output graph at motor speed 3

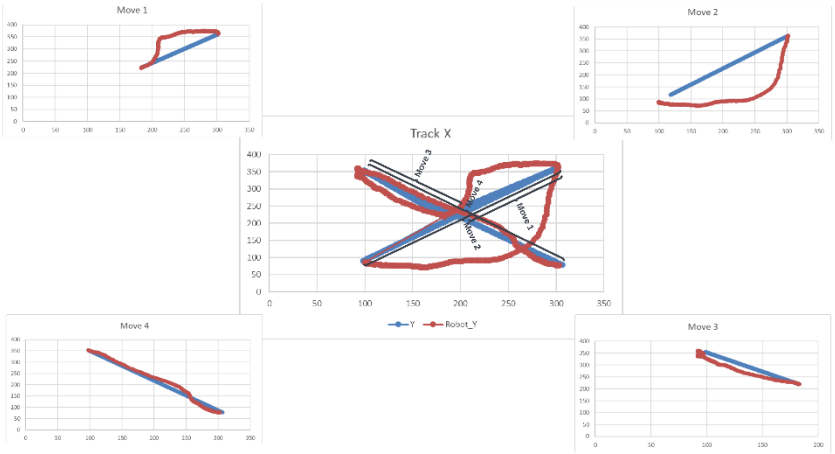

Fig. 2. Robot Motion "X"

As detailed in Table 1, the largest error occurred during the second movement, with a Mean Absolute Error (MAE) of 134.96 pixels, likely due to the longer path length and the complexity of maintaining stability when moving from the upper right to the lower left corner. The smallest error was observed in the third movement, with an MAE of 52.49 pixels, suggesting that shorter diagonal trajectories are easier for the robot to follow with greater precision. The first and fourth movements exhibited intermediate errors, with MAE of 68.88 pixels and 109.10 pixels, respectively, possibly due to variations in the robot's initial orientation and movement dynamics when navigating long versus short diagonal paths. Despite the overall average error of 91.36 pixels, indicating the robot followed the trajectory relatively well, there is still room for improvement, particularly in movements involving longer trajectories and sharper corners. The time required to complete the "X" trajectory was 1.07 minutes, indicating a relatively efficient process, but further refinements in navigation algorithms and motion control could reduce path errors.

Table 1. Error Track ”X”

No	Move Track “X”	Mean Absolute Error (MAE)
1	Move 1	68.88 pixels
2	Move 2	134.96 pixels
3	Move 3	52.49 pixels
4	Move 4	109.10 pixels
Average overall error		**91.36 pixels (18.53%)**
Time		**01.07 minute**

For the "square" pattern, depicted in Fig. 12, the movement was also divided into four segments: (1) a short vertical from the top-left to the bottom-right corner, (2) a long horizontal from the bottom-right to the bottom-left corner, (3) a short vertical from the bottom-left to the top-left corner, and (4) a long horizontal from the top-left to the top-right corner. The robot's actual path was recorded in red, while the expected path was shown in blue in Fig. 11. The average error for the "square" pattern was 83.17 pixels or a 16.02% deviation from the path generated by the software.

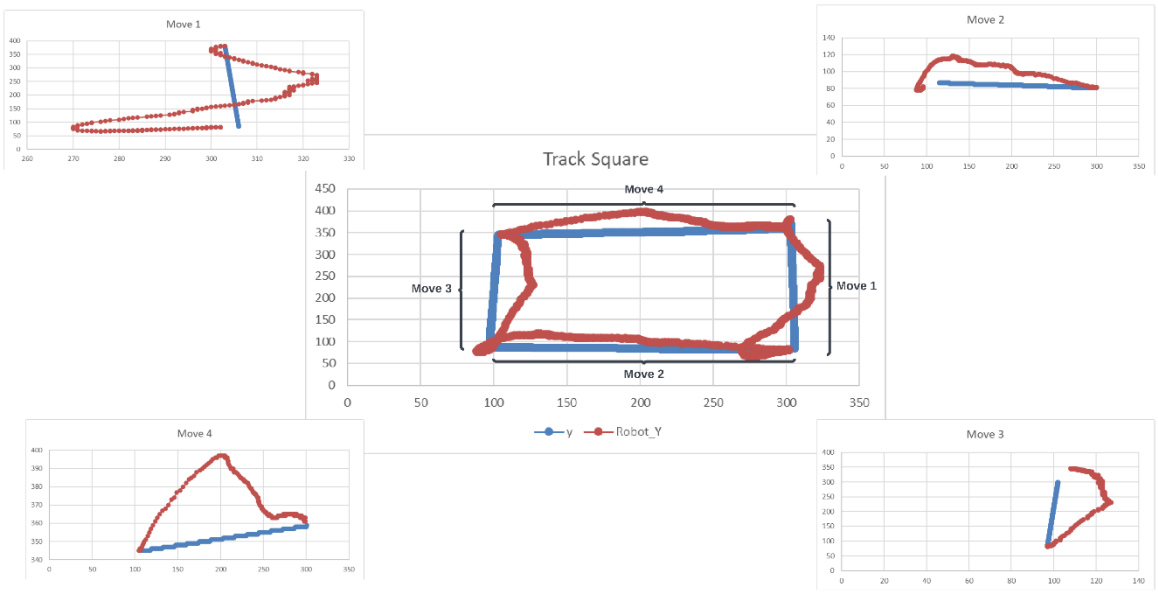

Fig. 3. Robot Motion ”Square”

Table 2 shows that the movements categorized as short vertical segments had higher errors than the longer horizontal segments. Specifically, the first movement had a Mean Absolute Error (MAE) of 105.37 pixels. This higher error could be attributed to the challenge of maintaining stability on short vertical paths, particularly when the robot adjusts its initial orientation. Similarly, the third movement, another short vertical segment, exhibited an MAE of 100.47 pixels, indicating a similar error pattern as the first movement.

Table 2. Error Track ”Square”

No	Move Track “Square”	Mean Absolute Error (MAE)
1	Move 1	105.37 pixels
2	Move 2	67.20 pixels
3	Move 3	100.47 pixels
4	Move 4	59.65 pixels
Average overall error		**83.17 pixels (16.02%)**
Time		**01.07 minute**

On the other hand, the second and fourth movements, which were longer horizontal segments, had lower errors, with MAE of 67.20 pixels and 59.65 pixels, respectively. The lower errors in these movements may be due to the robot having more space and time to make smoother and more stable adjustments over the extended horizontal paths.

Overall, the average error across all movements was 83.17 pixels, suggesting that while the robot generally followed the expected trajectory, further refinement is necessary, particularly in reducing errors during short vertical movements.

Visual control through an infrared camera and waypoint navigation yielded satisfactory results in guiding the robot along the expected paths. The infrared camera provided the necessary visual data to accurately determine the robot's position, while the waypoint navigation established reference points for the robot to follow. However, there is potential for further enhancements to improve both the accuracy and efficiency of the robot's movements. Implementing more advanced control algorithms and utilizing more precise sensors could help reduce errors, particularly in short vertical movements. Optimizing the waypoint navigation system could also enable smoother and more accurate trajectory navigation. Overall, these findings demonstrate that visual control and waypoint navigation are effective strategies for controlling omnidirectional robot movements, though there remains room for further optimization in movement accuracy and efficiency.

4. CONCLUSION

This research investigates the implementation of image-based position control on a Three-Wheel Omni-Directional Robot using waypoints to determine destination points. The robot is equipped with omnidirectional wheels, enhancing its maneuverability and flexibility in moving in various directions. Position control is achieved with an infrared camera mounted on the ceiling, enabling accurate detection and navigation based on the robot's detected position. The test results demonstrate that the robot can follow the expected trajectories with reasonable accuracy in both the "X" and "Square" tracks. In the "X" track, the second movement exhibited the largest error, with a Mean Absolute Error (MAE) of 134.96 pixels, while the third movement had the smallest error, with an MAE of 52.49 pixels. The overall average error of 91.36 pixels, or 18.53%, indicates that while the robot performs adequately, there is still room for improvement, particularly in navigating longer paths and sharp corners. In the "Square" track, the first and third movements had larger errors than the second and fourth movements, with MAE of 105.37 pixels and 100.47 pixels, respectively. In contrast, the second and fourth movements showed lower errors, with MAE of 67.20 pixels and 59.65 pixels. The average error of 83.17 pixels, or 16.02%, highlights the need for further refinement, especially in addressing errors in short vertical movements.

PID tuning significantly impacted the robot's movement. For instance, when the controller sends a command like (20, 20, 10) corresponding to motor speeds of 20 for motors 1 and 2 and 10 for motor 3, the robot is expected to move to a specific coordinate, such as (40, 50). However, due to suboptimal PID tuning, the actual motor speeds might deviate slightly (e.g., 19, 18, 7), causing the robot to reach a slightly different coordinate, such as (39, 51). This deviation results in longer times to reach the destination. Future work could improve PID tuning using machine learning algorithms such as Genetic Algorithms or Particle Swarm Optimization (PSO). Another source of error was the camera's low frame rate, which caused delays in capturing the robot's movements, making control more challenging. To mitigate this, the robot's maximum speed was reduced to allow the camera to keep up with its movements. Employing a higher frame rate camera could minimize these errors for future research. Additionally, the camera's susceptibility to external light sources compromised the reliability of robot detection in bright rooms or rooms with external light sources. Visual control with an infrared camera and waypoint navigation has proven to guide the robot along the expected paths in an indoor location. However, further improvements in the robot's control algorithms, such as fuzzy for keeping on the path and using more precise sensors, could help reduce errors and enhance the efficiency of the robot's movements. Optimizing the waypoint navigation system could also enable the robot to navigate trajectories more smoothly and precisely. Overall, this research demonstrates that integrating the superior maneuverability of omnidirectional wheeled robots with visual control capabilities using a camera holds significant potential in advancing modern robotics technology. This approach offers greater responsiveness and adaptability to the surrounding environment, with broad application potential across various industries.

REFERENCES

[1] A. S. Nath, "A Review of Advancements in Robotic and Sensor-based Technologies in Construction Sector," *European Journal of Engineering and Technology Research*, vol. 7, no. 1, 2022, http://dx.doi.org/10.24018/ejers.2022.7.1.2624.

[2] C. Fan, S. Wei, and Y. Yang, "Application of Multi-Sensor Fusion Precise Positioning and Autonomous Navigation Technology in Substation Intelligent Inspection Robot," in *Proceedings - 2024 International Conference on Electrical Drives, Power Electronics and Engineering, EDPEE*, pp. 624–629, 2024, https://doi.org/10.1109/EDPEE61724.2024.00122.

[3] J. Lin, Z. Miao, H. Zhong, W. Peng, Y. Wang, and R. Fierro, "Adaptive Image-Based Leader-Follower Formation Control of Mobile Robots with Visibility Constraints," *IEEE Transactions on Industrial Electronics*, vol. 68, no. 7, pp. 6010–6019, 2021, https://doi.org/10.1109/TIE.2020.2994861.

[4] F. Dong, D. Jin, X. Zhao, and J. Han, "Adaptive Robust Constraint following Control for Omnidirectional Mobile Robot: An Indirect Approach," *IEEE Access*, vol. 9, pp. 8877–8887, 2021, https://doi.org/10.1109/ACCESS.2021.3049913.
[5] R. L. Tiu *et al.*, "Development and Application of an Omni-Directional Robot for the Detection of Combustible and Toxic Gases," in *2021 IEEE 13th International Conference on Humanoid, Nanotechnology, Information Technology, Communication and Control, Environment, and Management, HNICEM*, pp. 1-6, 2021, https://doi.org/10.1109/HNICEM54116.2021.9732055.
[6] M. A. Riyadi, S. Rizqullah, S. Sumardi, and T. Prakoso, "Trajectory Tracking and Collision Avoidance on Smart Wheel Chair," *Jurnal Ilmiah Teknik Elektro Komputer dan Informatika*, vol. 8, no. 3, p. 354, 2022, https://doi.org/10.26555/jiteki.v8i3.24550.
[7] M. Zohaib, M. Ahsan, M. Khan, and J. Iqbal, "A featureless approach for object detection and tracking in dynamic environments," *PLoS One*, vol. 18, no. 1 2023, https://doi.org/10.1371/journal.pone.0280476.
[8] B. Y. Suprapto, A. Wahyudin, H. Hikmarika, and S. Dwijayanti, "The Detection System of Helipad for Unmanned Aerial Vehicle Landing Using YOLO Algorithm," *Jurnal Ilmiah Teknik Elektro Komputer dan Informatika*, vol. 7, no. 2, p. 193, 2021, https://doi.org/10.26555/jiteki.v7i2.20684.
[9] A. Saha and B. C. Dhara, "3D LiDAR-based obstacle detection and tracking for autonomous navigation in dynamic environments," *Int J Intell Robot Appl*, vol. 8, no. 1, pp. 39–60, 2024, https://doi.org/10.1007/s41315-023-00302-1.
[10] M. Auzan, R. M. Hujja, M. R. Fuadin, and D. Lelono, "Path Tracking and Position Control of Nonholonomic Differential Drive Wheeled Mobile Robot," *Jurnal Ilmiah Teknik Elektro Komputer dan Informatika*, vol. 7, no. 3, p. 368, 2021, https://doi.org/10.26555/jiteki.v7i3.21017.
[11] L. B. Soares *et al*., "Embedded System for Automation of Linear Welding Robot for Naval and Offshore Industry," in *IEEE International Conference on Industrial Informatics (INDIN)*, pp. 194–199, 2020, https://doi.org/10.1109/INDIN45582.2020.9442170.
[12] S. Guo, Q. Diao, and F. Xi, "Vision Based Navigation for Omni-directional Mobile Industrial Robot," *Procedia Comput Sci*, vol. 105, pp. 20–26, 2017, https://doi.org/10.1016/J.PROCS.20101.182.
[13] H. Zhu, H. Yang, M. Gao, Y. Liu, and Y. Li, "Mechanical environment analysis of non-stationary random excitation process of industrial robot," in *4th International Conference on Industrial Artificial Intelligence, IAI*, pp. 1-5, 2022, https://doi.org/10.1109/IAI55780.2022.9976677.
[14] Z. Wang *et al.*, "Field Calibration Method for Industrial Robots Based on Single Position Sensitive Device," *IEEE Trans Instrum Meas*, vol. 72, 2023, https://doi.org/10.1109/TIM.2023.3291734.
[15] S. Long, T. Terakawa, M. Komori, and T. Ougino, "Analysis of Traveling Strategies for Driving Omni-Wheeled Vehicle around a Corner," *IEEE Access*, vol. 8, pp. 104841–104856, 2020, https://doi.org/10.1109/ACCESS.2020.2999344.
[16] R. Barua, S. Mandal, and S. Mandal, "Motion Analysis of A Mobile Robot With Three Omni-Directional Wheels," *International Journal of Innovative Science, Engineering & Technology*, vol. 2, no. 11, pp. 644-648, 2015, https://ijiset.com/vol2/v2s11/IJISET_V2_I11_84.pdf.
[17] H. Taheri and C. X. Zhao, "Omnidirectional mobile robots, mechanisms and navigation approaches," *Mechanism and Machine Theory*, vol. 153, p. 103958, 2020, https://doi.org/10.1016/j.mechmachtheory.2020.103958.
[18] R. Vestman, "A Comparative Study of Omnidirectional and Differential Drive Systems for Mobile Manipulator Robots," Performance *Review of Strengths and Weaknesses*, 2023, https://www.diva-portal.org/smash/record.jsf?pid=diva2%3A1783655&dswid=-6607.
[19] C. Wang, X. Liu, X. Yang, F. Hu, A. Jiang, and C. Yang, "Trajectory tracking of an omni-directional wheeled mobile robot using a model predictive control strategy," *Applied Sciences (Switzerland)*, vol. 8, no. 2, 2018, https://doi.org/10.3390/app8020231.
[20] V. N. Kadam, L. Vachhani, and A. Gupta, "Control of an Omnidirectional Mobile Base with Multiple Spherical Robots," in *Sixth Indian Control Conference (ICC)*, pp. 350, 355, 2019, https://doi.org/10.1109/ICC47138.2019.9123198.
[21] X. Li, Y. Zhou, R. Guo, X. Peng, Z. Zhou, and H. Lu, "Spatio-Temporal Calibration for Omni-Directional Vehicle-Mounted Event Cameras," *IEEE Robot Autom Lett*, vol. 9, no. 3, pp. 2311–2318, 2024, https://doi.org/10.1109/LRA.2024.3355765.
[22] C. Hajdu, J. Hollosi, R. Krecht, A. Ballagi, and C. R. Pozna, "Economical Mobile Robot Design Prototype and Simulation for Industry 4.0 Applications," in CANDO-EPE 2020 - *Proceedings, IEEE 3rd International Conference and Workshop in Obuda on Electrical and Power Engineering*, pp. 155–160, 2020, https://doi.org/10.1109/CANDO-EPE51100.2020.9337786.
[23] N. Hacene and B. Mendil, "Motion Analysis and Control of Three-Wheeled Omnidirectional Mobile Robot," *Journal of Control, Automation and Electrical Systems*, vol. 30, no. 2, pp. 194–213, 2019, https://doi.org/10.1007/s40313-019-00439-0.
[24] O. Medina and S. Hacohen, "Overcoming kinematic singularities for motion control in a caster wheeled omnidirectional robot," *Robotics*, vol. 10, no. 4, 2021, https://doi.org/10.3390/robotics10040133.
[25] J. Liang, "Research on Industrial Robot Trajectory Tracking Control System based on PID Feedforward Algorithm," in *2022 IEEE 2nd International Conference on Electronic Technology, Communication and Information*, *ICETCI*, pp. 338–342, 2022, https://doi.org/10.1109/ICETCI55101.2022.9832315.
[26] F. Ribeiro, P. Silva, and N. Pereira, "Three omni-directional wheels control on a mobile robot," 2004, https://repositorium.sdum.uminho.pt/handle/1822/3293.

[27] C. Iaboni, H. Patel, D. Lobo, J. W. Choi, and P. Abichandani, "Event Camera Based Real-Time Detection and Tracking of Indoor Ground Robots," *IEEE Access*, vol. 9, pp. 166588–166602, 2021, https://doi.org/10.1109/ACCESS.2021.3133533.
[28] R. Jangir, N. Hansen, S. Ghosal, M. Jain, and X. Wang, "Look Closer: Bridging Egocentric and Third-Person Views with Transformers for Robotic Manipulation," *IEEE Robot Autom Lett*, vol. 7, no. 2, pp. 3046–3053, 2022, https://doi.org/10.1109/LRA.2022.3144512.
[29] X. Liang, H. Wang, Y. H. Liu, W. Chen, and Z. Jing, "Image-Based Position Control of Mobile Robots with a Completely Unknown Fixed Camera," *IEEE Trans Automat Contr*, vol. 63, no. 9, pp. 3016–3023, 2018, https://doi.org/10.1109/TAC.2018.2793458.
[30] R. Jangir, N. Hansen, S. Ghosal, M. Jain, and X. Wang, "Look Closer: Bridging Egocentric and Third-Person Views with Transformers for Robotic Manipulation," *IEEE Robot Autom Lett*, vol. 7, no. 2, pp. 3046–3053, 2022, https://doi.org/10.1109/LRA.2022.3144512.
[31] D. Zhao, F. Sun, Z. Wang, Q. Zhou, "A novel accurate positioning method for object pose estimation in robotic manipulation based on vision and tactile sensors," *The International Journal of Advanced Manufacturing Technology*, vol. 116, pp. 2999-3010, 2021, https://doi.org/10.1007/s00170-021-07669-0.
[32] K. Miatliuk, M. Pietrzak, and A. G. Buch, "Controlling an industrial robotic system based on received visual information," in *20th International Carpathian Control Conference (ICCC)*, 2019. http://doi.org/10.1109/CarpathianCC.2019.8765942.
[33] T. Barabas, H. Silaghi, D. Spoiala, and M. Gamcova, "Control System of an Autonomous Object Tracking Robot," in *2023 17th International Conference on Engineering of Modern Electric Systems, EMES,* 2023, https://doi.org/10.1109/EMES58375.2023.10171684.
[34] X. Liang, H. Wang, Y. H. Liu, B. You, Z. Liu, and W. Chen, "Calibration-Free Image-Based Trajectory Tracking Control of Mobile Robots with an Overhead Camera," *IEEE Transactions on Automation Science and Engineering*, vol. 17, no. 2, pp. 933–946, 2020, https://doi.org/10.1109/TASE.2019.2951714.
[35] S. Yasuda, T. Kumagai, and H. Yoshida, "Calibration-free Localization for Mobile Robots Using an External Stereo Camera," *2020 IEEE International Conference on Consumer Electronics (ICCE)*, pp. 1-6, 2020. https://doi.org/10.1109/ICCE46568.2020.9042969.
[36] Z. Li, Y. Yuan, F. Ke, W. He, and C. Y. Su, "Robust Vision-Based Tube Model Predictive Control of Multiple Mobile Robots for Leader-Follower Formation," *IEEE Transactions on Industrial Electronics*, vol. 67, no. 4, pp. 3096–3106, 2020, https://doi.org/10.1109/TIE.2019.2913813.
[37] Z. Miao, H. Zhong, Y. Wang, H. Zhang, H. Tan, and R. Fierro, "Low-Complexity Leader-Following Formation Control of Mobile Robots Using Only FOV-Constrained Visual Feedback," *IEEE Trans Industr Inform*, vol. 18, no. 7, pp. 4665–4673, 2022, https://doi.org/10.1109/TII.2021.3113341.
[38] Z. Chen, K. Zhang, Y. Huang, and X. Gao, "A Mobile Robot with the Functions of Visual Navigation and Digital Identification," in *2022 IEEE International Conference on Mechatronics and Automation, ICMA,* pp. 605–610, 2022, https://doi.org/10.1109/ICMA54519.2022.9856306.
[39] B. Sun, J. Wei, and X. Tang, "The Optimization of Object Detection and Localization in Complex Background for Vision-based Robot," in *Proceedings of 2020 IEEE International Conference on Integrated Circuits, Technologies and Applications, ICTA 2020*, pp. 176–177, 2020, https://doi.org/10.1109/ICTA50426.2020.9332115.
[40] R. Watiasih, M. Rivai, R. A. Wibowo, and O. Penangsang, "Path Planning Mobile Robot Using Waypoint For Gas Level Mapping," *IEEE, International Seminar on Intelligent Technology and Its Application*, pp. 244-249, 2017, https://doi.org/https://doi.org/10.1109/ISITIA.2017.8124088.
[41] M. Goutham, S. Boyle, M. Menon, S. Mohan, S. Garrow, and S. S. Stockar, "Optimal Path Planning Through a Sequence of Waypoints," *IEEE Robot Autom Lett*, vol. 8, no. 3, pp. 1509–1514, 2023, https://doi.org/10.1109/LRA.2023.3240662.
[42] A. Kamalova, K. D. Kim, and S. G. Lee, "Waypoint mobile robot exploration based on biologically inspired algorithms," *IEEE Access*, vol. 8, pp. 190342–190355, 2020, https://doi.org/10.1109/ACCESS.2020.3030963.
[43] A. Priyatmoko, I. Ardiyanto, and A. I. Cahyadi, "Dynamic Odometry for Waypoint Tracking of Omnidirectional Mecanum Wheeled Mobile Robot for Efficient Movement," in *ICITEE 2022 - Proceedings of the 14th International Conference on Information Technology and Electrical Engineering*, pp. 30–35, 2022, https://doi.org/10.1109/ICITEE56407.2022.9954102.
[44] M. Kamezaki, A. Kobayashi, R. Kono, M. Hirayama, and S. Sugano, "Dynamic Waypoint Navigation: Model-Based Adaptive Trajectory Planner for Human-Symbiotic Mobile Robots," *IEEE Access*, vol. 10, pp. 81546–81555, 2022, https://doi.org/10.1109/ACCESS.2022.3194146.
[45] A. Krishnan and P. Sudarshan, "Self-Localization and Waypoints following of Holonomic Three Wheeled Omni-Directional Mobile Robot," in *2021 IEEE International Conference on Distributed Computing, VLSI, Electrical Circuits and Robotics, DISCOVER 2021 - Proceedings*, pp. 253–258, 2021, https://doi.org/10.1109/DISCOVER52564.2021.9663644.
[46] M. R. Azizi, A. Rastegarpanah, and R. Stolkin, "Motion planning and control of an omnidirectional mobile robot in dynamic environments," *Robotics*, vol. 10, no. 1, 2021, https://doi.org/10.3390/robotics10010048.
[47] J. C. H. German, J. L. A. Alarcon, and S. R. P. Gardini, "Kinematic Modeling of a Mobile Robot with Four Tractor-Type Wheels with Independent Electric Drive," in *Proceedings of the 2023 IEEE 30th International Conference on Electronics, Electrical Engineering and Computing, INTERCON*, pp. 1-6, 2023. https://doi.org/10.1109/INTERCON59652.2023.10326042.

[48] A. S. Lafmejani *et al.*, "Kinematic modeling and trajectory tracking control of an octopus-inspired hyper-redundant robot," *IEEE Robot Autom Lett*, vol. 5, no. 2, pp. 3460–3467, 2020, https://doi.org/10.1109/LRA.2020.2976328.
[49] I. Siradjuddin, A. Junaidi, R. I. Putri, E. Rohadi, and S. Adhisuwignjo, "Kinematics and Control A Three Wheeled Omnidirectional Mobile Robot," *Int. J. Electr. Electron. Eng*, vol. 6, no. 12, pp. 1-6, 2019, https://www.internationaljournalssrg.org/IJEEE/2019/Volume6-Issue12/IJEEE-V6I12P101.pdf.
[50] H. Purnata, S. Ramadan, M. A. Hidayat, and I. Maulana, "PID Control Schematic Design for Omni-directional Wheel Mobile Robot Cilacap State of Polytechnic," *Journal of Telecommunication Network*, vol. 12, no. 2, 2022, https://garuda.kemdikbud.go.id/documents/detail/2869305.
[51] R. T. Yunardi, D. Arifianto, F. Bachtiar, and J. I. Prananingrum, "Holonomic implementation of three wheels omnidirectional mobile robot using DC motors," *Journal of Robotics and Control (JRC)*, vol. 2, no. 2, pp. 65–71, 2021, https://doi.org/10.18196/jrc.2254.
[52] G. Al *et al.*, "A General Inverse Kinematic Formulation and Control Schemes for Omnidirectional Robots," *Engineering Letters*, vol. 29, no. 1, 2022, https://www.engineeringletters.com/issues_v29/issue_4/EL_29_4_06.pdf.
[53] L. P. Truong, H. L. Tsai, and H. C. Tuan, "Development Of Directional Algorithm For Three- Wheel Omnidirectional Autonomous Mobile Robot," *Vietnam J Sci Technol*, vol. 59, no. 3, pp. 345–356, 2021, https://doi.org/10.15625/2525-2518/59/3/15583.
[54] M. Saad, A. H. Amhedb, and M. Al Sharqawi, "Real time DC motor position control using PID controller in LabVIEW," *Journal of Robotics and Control (JRC)*, vol. 2, no. 5, pp. 342–348, 2021, https://doi.org/10.18196/jrc.25104.
[55] M. H. Haider *et al.*, "Robust mobile robot navigation in cluttered environments based on hybrid adaptive neuro-fuzzy inference and sensor fusion," *Journal of King Saud University - Computer and Information Sciences*, vol. 34, no. 10, pp. 9060–9070, 2022, https://doi.org/10.1016/j.jksuci.2022.08.031.
[56] M. T. Ballestar, Á. Díaz-Chao, J. Sainz, and J. Torrent-Sellens, "Impact of robotics on manufacturing: A longitudinal machine learning perspective," *Technol Forecast Soc Change*, vol. 162, p. 120348, 2021, https://doi.org/10.1016/J.TECHFORE.2020.120348.
[57] A. J. Hammoodi, K. S. Flayyih, A. R. Hamad, "Design and implementation speed control system of DC Motor based on PID control and Matlab Simulink," *International Journal of Power Electronics and Drive System (IJPEDS),* 127, vol. 11, no. 1, pp. 127-134, 2019, https://doi.org/10.11591/ijpeds.v11.i1.pp127-134.
[58] R. Xiong, L. Li, C. Zhang, K. Ma, X. Yi, and H. Zeng, "Path Tracking of a Four-Wheel Independently Driven Skid Steer Robotic Vehicle Through a Cascaded NTSM-PID Control Method," *IEEE Trans Instrum Meas*, vol. 71, 2022, https://doi.org/10.1109/TIM.2022.3160549.

BIOGRAPHY OF AUTHORS

Sri Sukamta, Dosen Teknik Elektro, Departemen Pendidikan Teknik Elektro, Universitas Negeri Semarang, Indonesia. Bidang keahlian *Management Education, Electrical*, ssukamta2014@mail.unnes.ac.id and http://orcid.org/0000-0002-9238-1036.

Anan Nugroho, Dosen Teknik Elektro, Departemen Teknik Elektro, Universitas Negeri Semarang, Indonesia. Bidang keahlian *Signal and Image Processing*, *Computer Vision*, *Pattern Recognition*, anannugroho@mail.unnes.ac.id and http://orcid.org/0000-0002-3844-1405.

Subiyanto, Dosen Teknik Elektro, Departemen Teknik Elektro, Universitas Negeri Semarang, Indonesia. Bidang keahlian *artificial intelligent, electrical engineering*, subiyanto@mail.unnes.ac.id and http://orcid.org/0000-0001-5890-7017.

Rizal Rezianto, Mahasiswa Teknik Elektro, Departemen Pendidikan Teknik Elektro, Univeristas Negeri Semarang, Indonesia, rizalrezianto14@students.unnes.ac.id and http://orcid.org/0009-0005-4946-808X.

Muhammad Febrian Soambaton, Mahasiswa Teknik Elektro, Departemen Teknik Elektro, Univeristas Negeri Semarang, Indonesia, mfebriansoambaton@students.unnes.ac.id and http://orcid.org/0009-0009-8221-7046.

Agus Ardiyanto, Mahasiswa Teknik Elektro, Departemen Teknik Elektro, Univeristas Negeri Semarang, Indonesia, agusaa88@students.unnes.ac.id and http://orcid.org/0009-0004-7941-6355.